Article

Chiral three-dimensional supramolecular compounds: Homo and bimetallic oxalate and 1,2-dithiooxalate-bridged networks. A structural and photophysical study

DECURTINS, Silvio, *et al*.

Abstract

In analogy to the [MII(bpy)3]2+ cations, where MII is a divalent transition-metal and bpy is 2,2'-bipyridine, the tris-chelated [MIII(bpy)3]3+ cations, where MIII is CrIII or CoIII, induce the crystallization of chiral, anionic three-dimensional (3D) coordination polymers of oxalate-bridged (μ-ox) metal complexes with stoichiometries [MII2(ox)3]n2n- or [MIMIII(ox)3]n2n-. The tripositive charge is partially compensated by inclusion of additional complex anions like ClO4-, BF4-, or PF6- which are encapsulated in cubic shaped cavities formed by the bipyridine ligands of the cations. Thus, an elaborate structure of cationic and anionic species within a polymeric anionic network is realized. The compounds isolated and structurally characterized include [CrIII(bpy)3][ClO4] [NaCrIII(ox)3] (1), [CrIII(bpy)3][ClO4][MnII2(ox)3] (2), [CrIII(bpy)3][BF4] [MnII2(ox)3] (3), [CoIII(bpy)3][PF6][NaCrIII(ox)3] (4). Crystal data: 1, cubic, P213, a = 15.523(4) Å, Z = 4; 2, cubic, P4132, a = 15.564(3) Å, Z = 4; 3, cubic, P4132, a = 15.553(3) Å, Z = 4; 4, cubic, P213, a = 15.515(3) Å, Z = 4. Furthermore, it seemed likely that [...]

Reference

DECURTINS, Silvio, *et al*. Chiral three-dimensional supramolecular compounds: Homo and bimetallic oxalate and 1,2-dithiooxalate-bridged networks. A structural and photophysical study. *Inorganic chemistry*, 1996, vol. 35, no. 6, p. 1451-1460

DOI : 10.1021/ic950791j

Chiral, Three-Dimensional Supramolecular Compounds: Homo- and Bimetallic Oxalate- and 1,2-Dithiooxalate-Bridged Networks. A Structural and Photophysical Study†

Silvio Decurtins,*,‡ Helmut W. Schmalle,‡ René Pellaux,‡ Philippe Schneuwly,‡ and Andreas Hauser§

Institut für Anorganische Chemie, Universität Zürich, Winterthurerstrasse 190, CH-8057 Zürich, Switzerland, and Institut für Anorganische und Physikalische Chemie, Universität Bern, Freiestrasse 3, CH-3012 Bern, Switzerland

Received June 26, 1995⊗

In analogy to the $[M^{II}(bpy)_3]^{2+}$ cations, where M^{II} is a divalent transition-metal and bpy is 2,2′-bipyridine, the tris-chelated $[M^{III}(bpy)_3]^{3+}$ cations, where M^{III} is Cr^{III} or Co^{III}, induce the crystallization of chiral, anionic three-dimensional (3D) coordination polymers of oxalate-bridged (μ-ox) metal complexes with stoichiometries $[M^{II}_2(ox)_3]_n^{2n-}$ or $[M^{I}M^{III}(ox)_3]_n^{2n-}$. The tripositive charge is partially compensated by inclusion of additional complex anions like ClO_4^-, BF_4^-, or PF_6^- which are encapsulated in cubic shaped cavities formed by the bipyridine ligands of the cations. Thus, an elaborate structure of cationic and anionic species within a polymeric anionic network is realized. The compounds isolated and structurally characterized include $[Cr^{III}(bpy)_3][ClO_4]$ $[NaCr^{III}(ox)_3]$ (**1**), $[Cr^{III}(bpy)_3][ClO_4][Mn^{II}_2(ox)_3]$ (**2**), $[Cr^{III}(bpy)_3][BF_4]$ $[Mn^{II}_2(ox)_3]$ (**3**), $[Co^{III}(bpy)_3][PF_6][NaCr^{III}(ox)_3]$ (**4**). Crystal data: **1**, cubic, $P2_13$, $a = 15.523(4)$ Å, $Z = 4$; **2**, cubic, $P4_132$, $a = 15.564(3)$ Å, $Z = 4$; **3**, cubic, $P4_132$, $a = 15.553(3)$ Å, $Z = 4$; **4**, cubic, $P2_13$, $a = 15.515(3)$ Å, $Z = 4$. Furthermore, it seemed likely that 1,2-dithiooxalate (dto) could act as an alternative to the oxalate bridging ligand, and as a result the compound $[Ni^{II}(phen)_3][NaCo^{III}(dto)_3]\cdot C_3H_6O$ (**5**) has successfully been isolated and structurally characterized. Crystal data: **5**, orthorhombic, $P2_12_12_1$, $a = 16.238(4)$ Å, $b = 16.225(4)$ Å, $c = 18.371(5)$ Å, $Z = 4$. In addition, the photophysical properties of compound **1** have been investigated in detail. In single crystal absorption spectra of $[Cr^{III}(bpy)_3][ClO_4][NaCr^{III}(ox)_3]$ (**1**), the spin−flip transitions of both the $[Cr(bpy)_3]^{3+}$ and the $[Cr(ox)_3]^{3-}$ chromophores are observed and can be clearly distinguished. Irradiating into the spin-allowed $^4A_2 \rightarrow {}^4T_2$ absorption band of $[Cr(ox)_3]^{3-}$ results in intense luminescence from the ^2E state of $[Cr(bpy)_3]^{3+}$ as a result of rapid energy transfer processes.

Introduction

The role of dipositive, tris-chelated transition-metal bipyridine complexes as templates in the formation and crystallization of chiral, three-dimensional (3D) homo- and bimetallic oxalate-bridged networks is now well-established.[1,2] The topological, chemical and physical properties of the resulting polymeric frameworks are fascinating. In particular, the three-dimensional connectivity of spin-carrying centers as well as the chemical variability of the metal ions render these compounds valuable candidates for experimental and theoretical studies in the field of molecular-based magnetic materials.[3,4] Of further interest is the occurrence of a specific Δ- or Λ-helical chirality originating from the $(L\hat{}L)_3$-type of connectivity which is effective for the cations as well as for the building blocks of the 3D extended network. As a matter of fact, basically enantiomerically pure single crystals are obtained, although in a few cases merohedrically twinned single crystals have been observed. In any respect, it is certainly a rare case in inorganic chemistry that turns up with structural architectures of chiral, polymeric 3D compounds which can be crystallized.

Addressing and summarizing the topological features, one has to recall that the rigid, but still somewhat adaptable supramolecular structures can be described as cubic, 3-connected 10-gon nets (10,3), and accordingly they may be considered as the 3-connected analogs of the diamond net.[5] Figure 1 displays a stereoview of the topology of this (10,3) framework on one side schematically and on the other side in form of a section of a metal-oxalate network. The crystal structure of the homometallic compounds is appropriately described within the pair of the cubic enantiomorphous space groups $P4_132/P4_332$, whereas the crystal structure of the heterometallic compounds is refined within the cubic space group $P2_13$. Obviously, the regular connectivity of the metal ions within the network in combination with the 32 (D_3) molecular point group symmetry of the cationic templates favors a cubic crystal symmetry, although this is not a prerequisite for the realization of that special network topology. In fact, for a 1,2-dithiooxalate analog to the three-dimensional oxalate compounds (compound **5** in the present series), we also found an orthorhombic crystal symmetry to be in accordance with the given (10,3) network structure.

Furthermore, we have previously drawn attention to the possibility of an extensive variation of the metal ions for the $[M^{II}(bpy)_3]^{2+}$ cations as well as for the network stoichiometries

† Dedicated to Professor Hans Rudolf Oswald on the occasion of his 65th birthday.

‡ Universität Zürich.

§ Universität Bern.

⊗ Abstract published in *Advance ACS Abstracts,* February 15, 1996.

(1) Decurtins, S.; Schmalle, H. W.; Schneuwly, P.; Oswald, H. R. *Inorg. Chem.* **1993**, *32*, 1888.

(2) Decurtins, S.; Schmalle, H. W.; Schneuwly, P.; Ensling, J.; Gütlich, P. *J. Am. Chem. Soc.* **1994**, *116*, 9521.

(3) *Proceedings of the International Symposium on Chemistry and Physics of Molecular Based Magnetic Materials;* Iwamura, H., Itoh, K., Kinoshita, M., Eds.; Molecular Crystals and Liquid Crystals: Gordon & Breach: London, 1993.

(4) *Proceedings of the IV International Conference on Molecule-Based Magnets;* Miller, J. S., Epstein, A. J., Eds.; Molecular Crystals and Liquid Crystals; Gordon & Breach: London, 1995.

(5) Wells, A. F. *Structural Inorganic Chemistry*; Clarendon Press: Oxford, England, 1984.

0020-1669/96/1335-1451$12.00/0

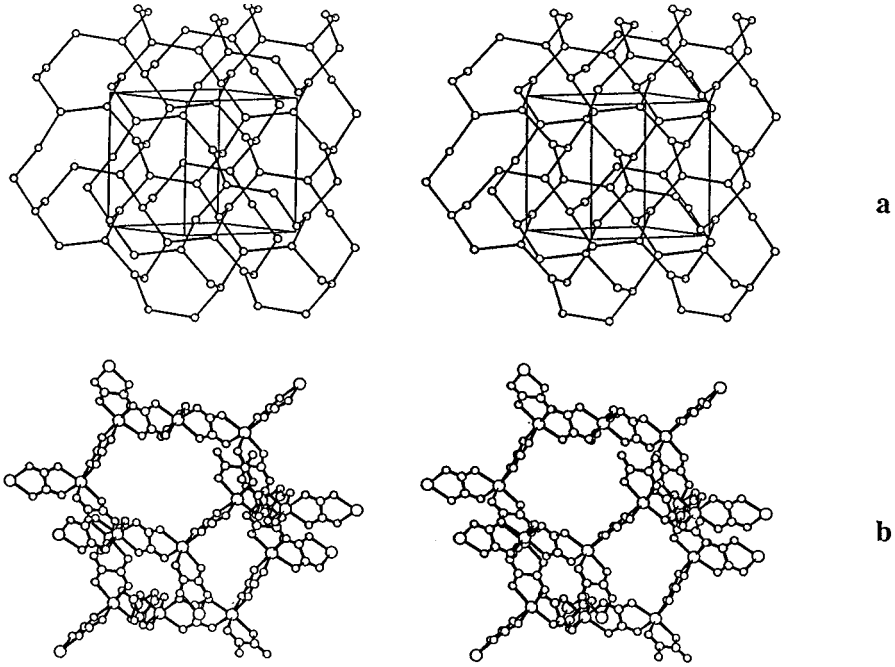

Figure 1. Stereoview of the 3-connected 10-gon (10,3) network topology (a), and of a section of a metal−oxalate network (b).

$[M^{II}_2(ox)_3]_n^{2n-}$ and $[M^{I}M^{III}(ox)_3]_n^{2n-}$. Now, in order to assess even in a more comprehensive way the chemical and structural flexibility of these networks and to expand our previous work, the tris-chelated cations which are belived to initiate the formation and crystallization of the nets, have been more extensively varied. On one side it is of interest to examine the structural response toward a $[M^{III}(bpy)_3]^{3+}$ template and on the other side toward a bulkier $[M^{II}(phen)_3]^{2+}$ cation, where phen is 1,10-phenanthroline. Surprisingly, in the former case, the system reacts with an elaborate inclusion of an additional complex anion while keeping the known topology, the crystal symmetry, and the lattice parameters fixed. It does so by encapsulating these anions in cubic-shaped empty spaces formed by six of the planar bipyridine ligands from three adjacent cations. In the latter case, as proven with the 1,2-dithiooxalate-bridged 3D compound (vide infra), the framework demonstrates a marked flexibility in adopting both the shape and width of the cavities to accommodate the steric requirements of the bulky cations.

Moreover, perceiving that 1,2-dithiooxalate may act as an alternative to the oxalate bridging ligand, we set the target to demonstrate that 1,2-dithiooxalate may build up the analogous polymeric three-dimensional networks. As a result, the crystal structure of a first example of a 3D dithiooxalate-bridged compound is reported.

Of further interest is the study of the photophysical properties of these systems. In this contribution we also report the results obtained from single-crystal absorption spectroscopy and from luminescence experiments carried out on compound **1**. The special advantage of the chosen metal ion combination for **1** is that it allows for an unequivocal observation of resonant and phonon-assisted energy transfer processes, on one side within the infinite donor array and on the other side between the donor and acceptor sites.

Experimental Section

Materials. Standard literature procedures were used to prepare the following complexes: $K_3[Cr(ox)_3]\cdot 3H_2O$,[6] $[Cr(bpy)_3][ClO_4]_3$,[7] $[Cr(bpy)_3][BF_4]_3$,[7] $[Co(bpy)_3][PF_6]_3$,[8] $[Ni(phen)_3][SO_4]$,[9] 1,2-dithiooxalate (dto),[10] and $K_3[Co(dto)_3]\cdot 2H_2O$.[11,12] The other reagents were obtained from commercial sources and were used as purchased. (*Caution!* Perchlorate salts of metal complexes can be explosive and must be handled with care.)

Single Crystal Growth of the Compounds 1−4. Deeply colored single crystals of both the homometallic network-type **2** and **3** and the heterometallic network-type **1** and **4** were grown with the gel technique according to the published procedure,[2] only replacing the $[M^{II}(bpy)_3]^{2+}$ salts by the chosen $[M^{III}(bpy)_3]^{3+}$ salts.

$[Cr^{III}(bpy)_3][ClO_4][NaCr^{III}(ox)_3]$ (1). An X-ray structural analysis was completed. Anal. Calcd for $C_{36}H_{24}ClCr_2N_6NaO_{16}$: C, 45.08; H, 2.52; N, 8.76; Cl, 3.70; Cr, 10.84; Na, 2.40. Found: C, 45.10; H, 2.50; N, 8.85; Cl, 3.70; Cr, 10.10; Na, 2.40.

$[Rh^{III}:Cr^{III}(1\%)(bpy)_3][ClO_4][NaCr^{III}(ox)_3]$. For the luminescence measurements, a microcrystalline precipitate was prepared according to the published procedure,[2] only replacing the $[M^{II}(bpy)_3]^{2+}$ salt by $[Rh^{III}(bpy)_3][ClO_4]_3$ with a 1% doping of $[Cr^{III}(bpy)_3][ClO_4]_3$. The X-ray powder diffraction data showed it to be structurally isomorphous to **1**.

$[Rh(bpy)_3][ClO_4]_3$. A 20 mL sample of a water/ethanol (50/50) solution containing 1 g of $RhCl_3\cdot 3H_2O$ and 2.4 g of 2,2′-bipyridine were refluxed for 24 h. After addition of charcoal, the suspension was refluxed for another hour and finally filtered to remove any solid particles. Upon addition of 20 mL of concentrated, aqueous $NaClO_4$ solution and cooling in an ice bath, the microcrystalline product was deposited. It was recrystallized from a water/ethanol (40/60) solution.

$[Cr^{III}(bpy)_3][ClO_4][Mn^{II}_2(ox)_3]$ (2). An X-ray structural analysis was completed. Anal. Calcd for $C_{36}H_{24}ClCrMn_2N_6O_{16}$: C, 43.50; H, 2.43; N, 8.46; Cl, 3.57; Cr, 5.23; Mn, 11.06. Found: C, 43.40; H, 2.30; N, 8.60; Cl, 3.70; Cr, 5.20; Mn, 10.50.

$[Cr^{III}(bpy)_3][BF_4][Mn^{II}_2(ox)_3]$ (3). An X-ray structural analysis was completed. Anal. Calcd for $C_{36}H_{24}BCrF_4Mn_2N_6O_{12}$: C, 44.06; H, 2.47; N, 8.56; Cr, 5.30; Mn, 11.20. Found: C, 42.90; H, 2.45; N, 8.35; Cr, 5.25; Mn, 10.85.

$[Co^{III}(bpy)_3][PF_6][NaCr^{III}(ox)_3]$ (4). An X-ray structural analysis was completed. Anal. Calcd for $C_{36}H_{24}CoCrF_6N_6NaO_{12}P$: C, 42.75; H, 2.39; N, 8.31; Co, 5.83; Cr, 5.14; Na, 2.27. Found: C, 42.70; H, 2.45; N, 8.55; Co, 5.95; Cr, 4.60; Na, 2.05.

(6) Bailar, J. C.; Jones, E. M. In *Inorganic Synthesis*; Booth, H. S., Ed.; McGraw-Hill: New York, 1939; Vol. 1, p 35.
(7) Baker, B. R.; Metha, B. D. *Inorg. Chem.* **1965**, *4*, 849.
(8) Burstall, F. H.; Nyholm, R. S. *J. Chem. Soc.* **1952**, 3570.
(9) Schilt, A. A.; Taylor, R. C. *J. Inorg. Nucl. Chem.* **1959**, *9*, 211.
(10) Jones, H. O.; Tasker, H. S. *J. Chem. Soc.* **1909**, 1904.
(11) Dwyer, F. P.; Sargeson, A. M. *J. Am. Chem. Soc.* **1959**, *81*, 2335.
(12) Dietzsch, W.; Strauch, P.; Hoyer, E. *Coord. Chem. Rev.* **1992**, *121*, 43.

Table 1. Crystallographic Data for Complexes **1**, **2**, **3**, **4**, and **5**

	1	**2**	**3**	**4**	**5**
formula	$C_{36}H_{24}ClCr_2NaN_6O_{16}$	$C_{36}H_{24}ClCrMn_2N_6O_{16}$	$C_{36}H_{24}BCrF_4Mn_2N_6O_{12}$	$C_{36}H_{24}CoCrF_6NaN_6O_{12}P$	$C_{45}H_{30}CoNaNiN_6O_7S_6$
fw	959.05	993.94	981.30	1011.50	1099.74
space group	$P2_13$ (No. 198)	$P4_132$ (No. 213)	$P4_132$ (No. 213)	$P2_13$ (No. 198)	$P2_12_12_1$ (No. 19)
a, Å	15.523(4)	15.564(3)	15.553(3)	15.515(3)	16.238(4)
b, Å					16.225(4)
c, Å					18.371(5)
V, Å^3	3741(2)	3770.2(13)	3762.2(13)	3734.7(13)	4840(2)
Z	4	4	4	4	4
T, K	295	295	295	295	295
calcd density, g cm^{-3}	1.703	1.751	1.732	1.799	1.509
obsd density, g cm^{-3}	1.69	1.73	1.71	1.79	1.50
λ, Å	0.710 73 (Mo)	0.710 73 (Mo)	0.710 73 (Mo)	0.710 73 (Mo)	0.710 73 (Mo)
μ, cm^{-1}	7.51	11.00	10.39	8.96	10.55
final R_1 and wR_2 indices based on F and F^2, $I > 2\sigma(I)$	0.050, 0.092	0.033, 0.066	0.047, 0.147	0.037, 0.095	0.087, 0.201
R_1 and wR_2 indices (all data)	0.180, 0.136	0.235, 0.131	0.096, 0.180	0.058, 0.113	0.259, 0.302

[a] R_1 factor definition: $R_1 = \sum||F_o| - |F_c||/\sum|F_o|$. SHELXL-93 w$R_2$ factor definition: $wR_2 = [\sum w(F_o^2 - F_c^2)^2/\sum w(F_o^2)^2]^{1/2}$. Weighting scheme: $w = 1/[\sigma^2(F_o)^2 + (np)^2 + 0.00p]$, $p = (\max(F_o^2) + 2F_c^2)/3$.

Preparation of $[Ni^{II}(phen)_3][NaCo^{III}(dto)_3]\cdot C_3H_6O$ (5). A water/acetone (50/50) solution of $K_3[Co(dto)_3]\cdot 2H_2O$ (0.005 M) was combined with a stoichiometric water/acetone (50/50) solution of $[Ni(phen)_3][SO_4]$ and NaCl. The resulting mixture was kept protected from light in a covered beaker to prevent the solvent from evaporation. Within several days, complex-shaped, deeply colored single crystals formed, and an X-ray structural analysis was completed. Anal. Calcd for $C_{45}H_{30}CoN_6NaNiO_7S_6$: C, 49.15; H, 2.75; N, 7.64; S, 17.49; Co, 5.36; Na, 2.09; Ni, 5.34. Found: C, 48.35; H, 3.25; N, 7.75; S, 18.70; Co, 5.20; Na, 2.10; Ni, 5.60.

Crystallographic Structure Determination. Some relevant crystallographic data and structure determination parameters for the four cubic (**1**, **2**, **3**, **4**) 3D structures and the orthorhombic 3D structure (**5**) are given in Table 1. Data for all five compounds were collected on an Enraf-Nonius CAD-4 diffractometer using graphite-monochromatized Mo Kα radiation. Unit cell parameters were obtained from least-squares refinement of the θ angles of 25 reflections with $12.0° < 2\theta < 37.0°$ for **1**; $14.6° < 2\theta < 31.8°$ for **2**; $15.2° < 2\theta < 31.8°$ for **3**; $15.4° < 2\theta < 21.2°$ for **4**; and $15.0° < 2\theta < 28.0°$ for **5**. Friedel pairs were collected in the ranges $1.85° < \theta < 20°$ for **1**; $1.85° < \theta < 21°$ for **3**; and $1.85° < \theta < 20°$ for **4**. The maximum θ values for the data collection were 30° for **1**, 32° for **2**, 30° for **3**, and 30° for **4**. Due to relatively large unit cell parameters, only a quarter of the limiting sphere was used for the data collection of compound **5** ($\theta_{max} = 28°$). It should be noted that the data reduction for compounds **1** and **4** is based on 3-fold equivalent measured reflections according to the lower symmetry of the space group $P2_13$, while for compounds **2** and **3** 6-fold measured equivalent reflections were reduced. The number of measured and unique reflections with R_{int} were 8026, 2505, and 0.076 for **1**; 13902, 2195, and 0.068 for **2**; 8234, 1838, and 0.048 for **3**; 8023, 2503, and 0.033 for **4**; and 12432, 11649, and 0.057 for **5**. The number of reflections with $I > 2\sigma(I)$ used to determine the lower R values in Table 1 are 1193 for **1**; 726 for **2**; 1232 for **3**; 1997 for **4**; 5361 for **5**. Data collection, unit cell refinement and crystal face indexing for absorption corrections were carried out with the Enraf-Nonius CAD-4 software.[13] Three standard reflections were measured every 3 h during the data collection for **1**−**4**. For compound **5** only two standard reflections were remeasured every 3 h. The observed decay and the number of measured standard reflections were −0.3%, 90 for **1**; −1.9%, 132 for **2**; −2.1%, 120 for **3**; −4%, 99 for **4**; and −0.2%, 82 for **5**. Absorption corrections are based on four (**1**), nine (**2**), eight (**3**), four (**4**), and 14 (**5**) indexed and measured crystal faces. Tetrahedral forms for **1** and **4** found by indexing the crystal faces are {111}. One corner of the octahedron of **2** appeared to be truncated and showed the crystal face (100). Compound **5** showed a complex morphology. Absolute structure parameters with their statistical uncertainities (su) and further experimental details are given in Table S14 (Supporting Information).

All five structures were solved by direct methods using SHELXS-86.[14] Space groups were determined by systematic extinction rules and by Flack's absolute structure parameter refinement.[15] No twinning by merohedry was noted for all five compounds. Refinements were performed on all five structures with SHELXL93[16] using anisotropic displacement parameters for all non-hydrogen atoms, except for the disordered perchlorate oxygen atoms in **1** (in **2** the perchlorate was refined anisotropically), the disordered BF_4^- group in **3**, and the disordered fluorine atoms of the PF_6^- group in **4**. All disordered groups in **1**−**4** have in common that the central atoms (Cl, B, P) occupy the sites with symmetry 32 (Wyckoff letter a) for **2** and **3** and sites with symmetry 3 (Wyckoff letters a or b) for **1** and **4**. In case of the ClO_4^- groups, one oxygen atom is situated within a 3-fold axis in $P4_132$, and two oxygen atoms are also located in the 3-fold axis in $P2_13$, whereas the other oxygen atoms are found in general positions. Altogether, two ($P4_132$) or four ($P2_13$) oxygen atoms were refined. Compared to these tetrahedral perchlorate groups, the BF_4^- and PF_6^- groups were found to be more disordered.

For compound **5**, not only the acetone group (which was isotropically refined with DFIX distance restraints) but also one of the dithiooxalate groups appeared to be strongly disordered. Split positional refinement trials of the disordered dithiooxalate group, as proposed by the program SHELXL93, were not stable at all. Even DFIX refinements, executed with averaged restrained bond distances C−O, C−S, and C−C were not successful. As the refined geometry of the unrestrained disordered ligand could also be interpreted as a trans-conformation according to the C−X (X = S or O) distances, a refinement for this kind of model, interchanging the O and S scattering factors for these positions, was also tried. However, temperature parameters indicated a clear preference for the cis-conformation. As no restraint model refined successfully, the disordered dithiooxalate group was finally refined freely as it appeared in the difference Fourier map. It remains an open question if the recently published result using a nonlinear least-squares procedure[17] could help to refine the disordered ligand adequately.

H atoms of the bipyridine ligands were included in calculated positions and refined as riding models with fixed U_{iso} at 1.2 U_{eq} values of the preceding normal atom, for compounds **1** and **2**. For compounds **3** and **4** however, the H atoms of the bipyridine part of the structures were fully refined with individual isotropic displacement parameters. Due to the larger number of symmetry independent ligands of the cation in **5**, the 24 phenanthroline H atoms were included at calculated sites (C−H = 0.93 Å) and were treated as the H atoms in **1** and **2**.

Optical Measurements. Single crystal absorption spectra of $[Cr^{III}(bpy)_3][ClO_4][NaCr^{III}(ox)_3]$ (**1**) were recorded with a Cary 5e

(13) Enraf-Nonius CAD-4 Software, Version 5.0, Enraf-Nonius, Delft, The Netherlands, 1989.

(14) Sheldrick, G. M. *Acta Crystallogr.* **1990**, *A46*, 467.
(15) Flack, H. D. *Acta Crystallogr.* **1983**, *A39*, 876.
(16) Sheldrick, G. M. Program for Crystal Structure Refinement. University of Göttingen, Germany, 1993.
(17) Spengler, R.; Lange, J.; Zimmermann, H.; Burzlaff, H. *Acta Crystallogr.* **1995**, *B51*, 174.

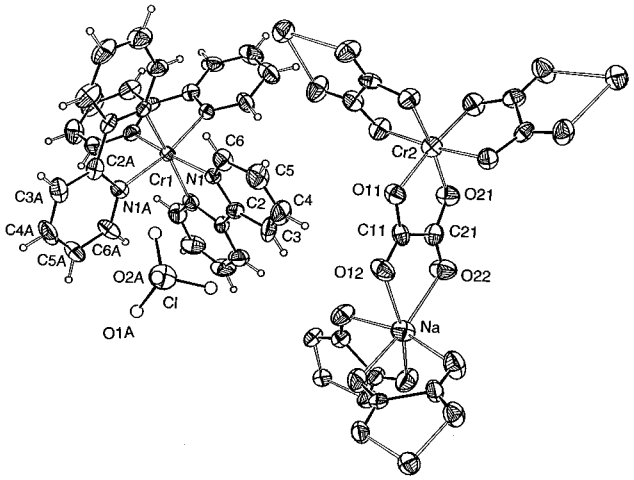

Figure 2. ORTEP drawing (50% probability level) with the labeling scheme of the asymmetric unit of $[Cr^{III}(bpy)_3][ClO_4][NaCr^{III}(ox)_3]$ (**1**). H- atoms are shown as spheres of arbitrary size.

Table 2. Fractional Coordinates ($\times 10^4$) and Equivalent Isotropic Displacement Parameters ($Å^2 \times 10^3$) for **1**

	x	*y*	*z*	$U_{(eq)}{}^a/U_{(iso)}{}^b$
Cr(1)	8740(1)	8740(1)	8740(1)	23(1)
N(1)	8713(3)	7425(3)	8851(3)	23(1)
C(2)	8719(4)	7123(4)	9670(4)	29(2)
C(3)	8682(4)	6250(4)	9840(5)	44(2)
C(4)	8641(5)	5676(4)	9158(6)	51(2)
C(5)	8639(5)	5983(5)	8325(5)	50(2)
C(6)	8687(4)	6863(4)	8199(5)	37(2)
N(1A)	8770(3)	8609(3)	10051(3)	29(1)
C(2A)	8763(4)	7785(4)	10344(4)	31(2)
C(3A)	8792(5)	7609(4)	11219(4)	43(2)
C(4A)	8855(5)	8286(6)	11793(4)	52(2)
C(5A)	8864(5)	9118(5)	11486(4)	49(2)
C(6A)	8825(5)	9254(5)	10619(4)	40(2)
Na	8460(2)	3460(2)	11540(2)	43(1)
Cr(2)	6033(1)	3967(1)	8967(1)	34(1)
O(11)	7290(3)	3867(3)	9075(3)	34(1)
O(21)	6057(3)	3912(3)	10226(3)	39(1)
C(11)	7559(4)	3741(4)	9847(4)	30(2)
C(21)	6802(4)	3750(5)	10547(4)	34(2)
O(12)	8298(3)	3638(4)	10065(3)	44(1)
O(22)	6977(3)	3592(3)	11292(3)	50(1)
Cl	11246(1)	6246(1)	8754(1)	56(1)
O(1A)	10699(11)	5699(11)	9301(11)	113(0)^b
O(2A)	11619(12)	5698(10)	8131(10)	104(5)^b
O(1B)	11779(12)	6779(12)	8221(12)	124(10)^b
O(2B)	10820(11)	5615(9)	8215(10)	93(5)^b

^{a} U(eq) is defined as one-third of the trace of the orthogonalized $\mathbf{U}_{ij}$ tensor. ^{b} Isotropically refined atoms.

Table 3. Selected Bond Lengths (Å) and Angles (deg) for **1**

Distances			
Cr(1)−N(1)	2.048(4) 3×	N(1A)−C(2A)	1.358(7)
Cr(1)−N(1A)	2.046(5) 3×	C(2A)−C(3A)	1.385(9)
		C(3A)−C(4A)	1.381(9)
Cr(2)−O(11)	1.964(4) 3×	C(4A)−C(5A)	1.377(10)
Cr(2)−O(21)	1.956(4) 3×	C(5A)−C(6A)	1.363(8)
Na−O(12)	2.320(6) 3×	O(11)−C(11)	1.283(7)
Na−O(22)	2.342(5) 3×	O(21)−C(21)	1.284(8)
		C(11)−O(12)	1.207(8)
N(1)−C(6)	1.338(8)	C(21)−O(22)	1.212(8)
N(1)−C(2)	1.354(8)	C(11)−C(21)	1.601(8)
C(2)−C(3)	1.383(9)		
C(2)−C(2A)	1.468(8)	Cl−O(1A)	1.47(3)
C(3)−C(4)	1.385(10)	Cl−O(2A)	1.41(2) 3×
C(4)−C(5)	1.378(10)	Cl−O(1B)	1.43(3)
C(5)−C(6)	1.381(9)	Cl−O(2B)	1.45(2) 3×
N(1A)−C(6A)	1.337(8)		

Angles			
$N(1A)^i$−Cr(1)−N(1A)	94.5(2) 3×	N(1A)−C(2A)−C(3A)	120.9(6)
N(1A)−Cr(1)−$N(1)^i$	93.0(2) 3×	N(1A)−C(2A)−C(2)	114.9(5)
N(1A)−Cr(1)−N(1)	79.5(2) 3×	C(3A)−C(2A)−C(2)	124.2(6)
$N(1)^i$−Cr(1)−N(1)	93.8(2) 3×	C(4A)−C(3A)−C(2A)	119.0(7)
N(1A)−Cr(1)−$N(1)^{ii}$	170.8(2) 3×	C(5A)−C(4A)−C(3A)	119.4(6)
		C(6A)−C(5A)−C(4A)	119.1(7)
$O(21)^v$−Cr(2)−O(21)	93.6(2) 3×	N(1A)−C(6A)−C(5A)	122.6(7)
$O(21)^v$−Cr(2)−O(11)	92.1(2) 3×		
O(21)−Cr(2)−O(11)	83.8(2) 3×	C(11)−O(11)−Cr(2)	114.5(4)
O(21)−Cr(2)−$O(11)^v$	173.9(2) 3×	C(21)−O(21)−Cr(2)	114.5(4)
O(11)−Cr(2)−$O(11)^v$	90.8(2) 3×	O(12)−C(11)−O(11)	126.3(6)
		O(12)−C(11)−C(21)	120.5(6)
$O(12)^{iii}$−Na−O(12)	90.1(2) 3×	O(11)−C(11)−C(21)	113.2(6)
$O(12)^{iii}$−Na−O(22)	92.8(2) 3×	O(22)−C(21)−O(21)	127.8(6)
O(12)−Na−O(22)	73.8(2) 3×	O(22)−C(21)−C(11)	118.7(6)
O(12)−Na−$O(22)^{iii}$	163.6(2) 3×	O(21)−C(21)−C(11)	113.4(5)
O(22)−Na−$O(22)^{iii}$	103.5(2) 3×	C(11)−O(12)−Na	113.4(4)
		C(21)−O(22)−Na	113.3(4)
C(6)−N(1)−C(2)	118.9(5)		
C(6)−N(1)−Cr(1)	125.9(4)	$O(2A)^{iii}$−Cl−$O(2A)^{iv}$	112.3(6)
C(2)−N(1)−Cr(1)	115.1(4)	$O(2A)^{iii}$−Cl−O(2A)	112.3(6)
N(1)−C(2)−C(3)	121.3(6)	$O(2A)^{iv}$−Cl−O(2A)	112.3(6)
N(1)−C(2)−C(2A)	115.3(5)	O(1B)−Cl−$O(2B)^{iii}$	108.7(6)
C(3)−C(2)−C(2A)	123.5(6)	O(1B)−Cl−O(2B)	108.7(6)
C(2)−C(3)−C(4)	119.1(7)	$O(2B)^{iii}$−Cl−O(2B)	110.2(6)
C(5)−C(4)−C(3)	119.7(7)	O(1B)−Cl−$O(2B)^{iv}$	108.7(6)
C(4)−C(5)−C(6)	118.3(8)	$O(2B)^{iii}$−Cl−$O(2B)^{iv}$	110.2(6)
N(1)−C(6)−C(5)	122.7(7)	O(2B)−Cl−$O(2B)^{iv}$	110.2(6)
		$O(2A)^{iii}$−Cl−O(1A)	106.5(6)
C(6A)−N(1A)−C(2A)	119.0(5)	$O(2A)^{iv}$−Cl−O(lA)	106.5(6)
C(6A)−N(1A)−Cr(1)	125.7(4)	O(2A)−Cl−0(1A)	106.5(6)
C(2A)−N(1A)−Cr(1)	115.2(4)		

^{a} Symmetry transformations used to generate equivalent atoms: (i) y, z, x; (ii) z, x, y; (iii) $y + {}^1/_2, -z + {}^3/_2, -x + 2$; (iv) $-z + 2, x - {}^1/_2, -y + {}^3/_2$; (v) $-y + 1, z - {}^1/_2, -x + {}^3/_2$; (vi) $-z + {}^3/_2, -x + 1, y + {}^1/_2$.

spectrophotometer. For this purpose, one corner of one of the perfectly tetrahedral crystals was polished off, using Al_2O_3 powder suspended in paraffin oil. The resulting triangular crystal (edges 0.4 mm, thickness 0.14 mm) was mounted on a piece of copper foil having an appropriate aperture. The copper foil, in turn, was inserted into an Air Products closed cycle cryostat capable of achieving temperatures down to 12 K. Luminescence measurements on **1** and on $[Rh^{III}:Cr^{III}(1\%)(bpy)_3][ClO_4][NaCr^{III}(ox)_3]$ were performed by irradiating powdered samples in quartz capillaries with the 568 nm line (2 mW CW) of a Kr^+ laser (Coherent Innova 300). The emitted light was dispersed with a ${}^3/_4$ m double monochromator (Spex 1404, gratings blazed at 500 nm, 1200 g/mm) and detected with a cooled GaAs photomuliplier (RCA C31034) in conjunction with a photon counting system (Standford Research SR 400). Sample temperatures down to 6.5 K were achieved using a cold He gas flow technique in order to ensure efficient cooling.

Results and Discussion

General Description of the Structures 1−4. The most notable feature of the structures **1**−**4** is the finding that the $[M^{III}(bpy)_3]^{3+}$ cations, like their dipositive analogous, are able to initiate the crystallization of chiral, polymeric 3D structures. Indeed, the successful structural analysis disclosed exactly the same network configurations and the same crystal packing arrangements between the cations and the extended anionic array as those which have been determined in the case of the dipositive cations.[1,2] Accordingly, both types of anionic networks, $[Mn^{II}_2(ox)_3]_n{}^{2n-}$ (**2**), (**3**) and $[NaCr^{III}(ox)_3]_n{}^{2n-}$ (**1**), (**4**), form basically the analogous three-dimensional pattern, namely 3-connected 10-gon nets (10,3). Thus, for a detailed discussion and an overall representation of these features, we may refer to the earlier reports.[1,2]

In this paper, compound **1** has been chosen for a photophysical study and a discussion of the different possible Cr(III) ↔ Cr(III) energy transfer processes. Therefore, a short crystallographic characterization is presented for **1**: Figure 2 shows an ORTEP drawing including both Cr(III) coordinations, and Tables 2 and 3 summarize the atomic fractional coordinates and

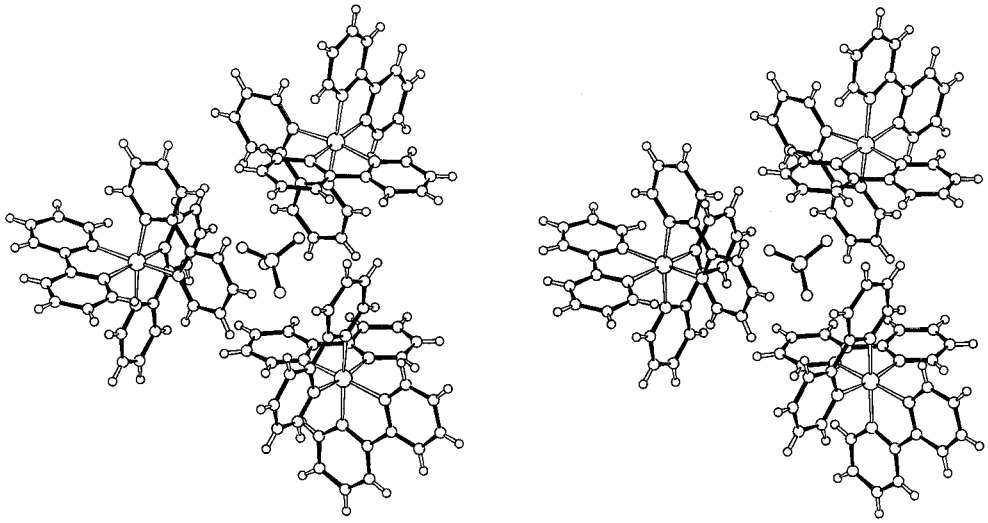

Figure 3. SCHAKAL stereodrawing of three adjacent $[Cr(bpy)_3]^{3+}$ complexes (**2**) exhibiting the cavity formed by three pairs of parallel oriented bipyridine ligands. The center of the cage is occupied by a $[ClO_4]^-$ anion.

selected bond lengths and angles. The corresponding data for compounds **2**−**4** are available as Supporting Information. The geometric values of the bridging oxalate ligands and of the metal coordination spheres compare well with those described in the analogous compounds with the same connectivity. Likewise, for a detailed discussion we may refer to these reports.[1,2,18]

New Structural Effects Originating from the Tripositive Templates. Herein we will concentrate on the new structural feature originating from the templation by the tripositive cations as it is demonstrated in case of compounds **1**−**4**. At first, one might anticipate that $[M(bpy)_3]^{3+}$ cations should, in principle, be able to initiate a crystallization of 3D networks with a new $[M^IM^{II}(ox)_3]_n^{3n-}$ framework stoichiometry. Alternatively, one could consider a structure which maintains the already known combinations of the metal oxidation states within the extended array, namely $[M^IM^{III}(ox)_3]_n^{2n-}$ or $[M^{II}_2(ox)_3]_n^{2n-}$. Consequently, in that case, an additional anion per formula unit would be needed to establish the charge balance.

During the course of our studies we learned that a clear selectivity exists in that only the latter case could be realized. Thus, the question arose as to where the required additional anions would fit into the elaborate crystal packing arrangement. Molecular modeling examinations revealed no favorable empty spaces between the cations and the surrounding anionic network as they share common surfaces in close contact. Nevertheless, a simple solution emerged when it was recognized that the special packing arrangement of the cations themselves with their three-bladed propellers from the bipyridine ligands create as well cubic-shaped cavities just large enough to accommodate the required additional anions. In particular, within the cubic space groups $P4_132/P4_332$ and $P2_13$, the tris-chelated cations are assembled in a specific and highly symmetrical manner, such that in all three directions a pairing of parallel aligned, adjacent bipyridine ligands occurs. Three of these pairs together, perpendicularly oriented to each other, form cubic shaped vacancies with ample space for encapsulating neutral or charged molecules. It is noteworthy that so far in none of the preparations from aqueous solution, any enclosure of water molecules has been found to take place. These findings should not be a surprise, taking into consideration the hydrophobic environment of these cavities. However, in the actual case of the structures **1**−**4**, the accumulation of positive charge from the tripositive cations results in an attractive Coulomb force strong enough to encapsulate anionic species.

Because each tris-chelated cation participates in the formation of three adjacent cavities, the target stoichiometry in a 1:1 ratio for the cation to encapsulated anion is realized with a full occupation of these vacancies. An examination of the site symmetry for these cavities, and hence the site symmetry for the hosted anions, reveals that there is a crystallographically imposed symmetry in form of a 3-fold axis. Figure 3 exhibits, as a stereodrawing, the packing arrangement of three adjacent tris-chelated cations (compound **2** is chosen as an example) together with the entrapped $[ClO_4]^-$ anion at the center of the cavity. The anion is shown in one of the two split positions which have been found in the structure refinement. Naturally, its molecular tetrahedral symmetry matches the crystallographically imposed C_3-axis well. Figures 4 and 5 are space-filling representations of the same structural environment as shown in Figure 3. Whereas Figure 4 beautifully accentuates the tight packing mode of the whole assembly, Figure 5 focuses on the regularly, cubic shaped cavity which is drawn with the frontal bipyridine ligand partially omitted in order to have a free view into the cage.

The diameter (plane to plane) of the cubic cavities for the compounds **1**−**4** is half of the corresponding unit cell axis; thus, a mean value of 7.77 Å may be quoted. Taking 1.85 Å for the half-thickness of the aromatic bipyridine ligand, there remains a spherical free space of about 4.1 Å in diameter to host the anion therein. The radius of a circumscribed sphere of $[ClO_4]^-$ is given as 2.90 Å;[19] consequently, there is no possibility for a rotational disorder and instead the oxygen atoms are confined to the directions of the vertices of the cube, again in accordance with the 3-fold symmetry axis. Thus, it is apparent that the encapsulated anion approaches the central metal atoms in the interligand pockets very closely. In particular, the Cr−O distance with a value of 4.25 Å is less than the cited value of 4.5 Å in the case of the tight ion pairs in $[Cr(terpy)_2][ClO_4]_3 \cdot H_2O$, terpy = 2,2′,2″-terpyridine.[19]

Description of the Structure $[Ni^{II}(phen)_3][NaCo^{III}(dto)_3] \cdot C_3H_6O$ (5). The topology of this compound shows the expected chiral three-dimensional (10,3) network configuration. In contrast to the corresponding 3D oxalate-bridged structures, which are described in cubic space groups, it is noteworthy that compound **5**, whose crystal structure was refined in the orthorhombic space group $P2_12_12_1$, shows all atoms to occupy only general positions. In particular, there is no more a crystallographically imposed 3-fold axis for the tris-chelated

(18) Decurtins, S.; Schmalle, H. W.; Oswald, H. R.; Linden, A.; Ensling, J.; Gütlich, P.; Hauser, A. *Inorg. Chim. Acta* **1994**, *216*, 65.

(19) Wickramasinghe, W. A.; Bird, P. H.; Serpone, N. *Inorg. Chem.* **1982**, *21*, 2694.

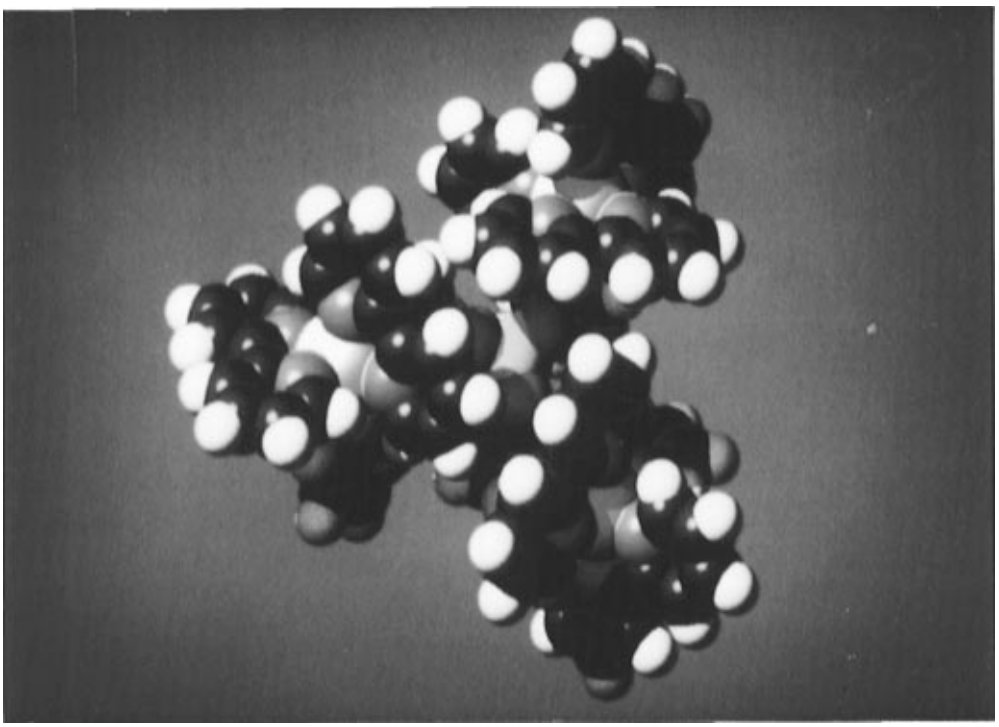

Figure 4. Space-filling model, accentuating the packing mode of the three adjacent $[Cr(bpy)_3]^{3+}$ cations encapsulating the perchlorate anion in **2**.

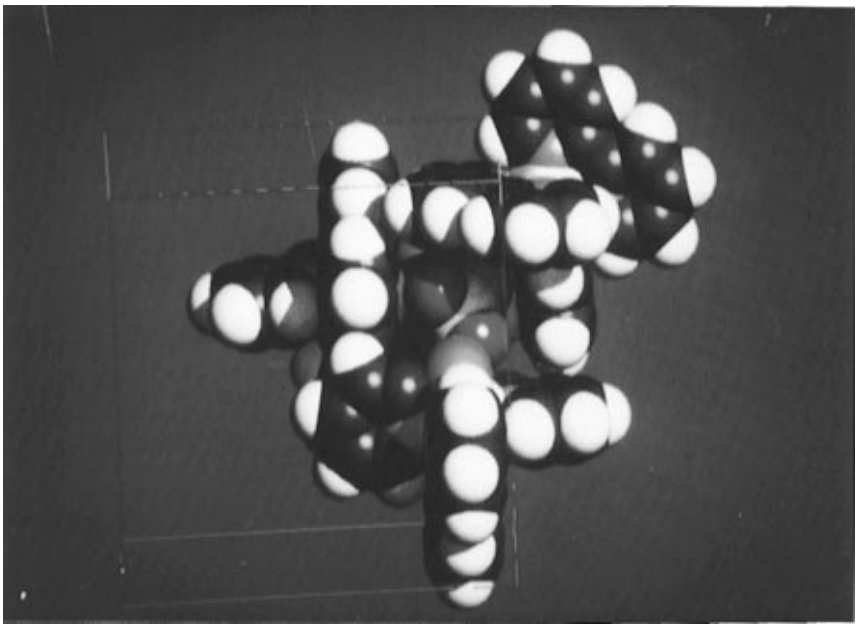

Figure 5. View along [100] of the same cubic shaped box as shown in Figure 4 (compound **2**). One half of the bipyridine ligand in front is omitted to show the hosted perchlorate anion.

metal ions, neither within the network nor for the cations. It should be noted that in spite of the nearly equal *a* and *b* axes, no tetragonal symmetry (e.g. $P4_12_12$ or $P4_32_12$) was observed.

A detailed illustration of the geometry of the Na, Co and Ni coordination, together with the labeling scheme of the asymmetric unit, is given in Figure 6. The atomic fractional coordinates and the principal bond lengths and angles are listed in Tables 4 and 5. A key structural element is certainly the specific coordination behavior of the bridging 1,2-dithiooxalate ligand. Evidently, a discrimination occurs, such that the bonding to cobalt(III) is through the sulfur atoms, whereas the sodium atoms bind to the oxygen ends of the bridging ligand.

The 1,2-dithiooxalate ligands are approximately planar. The dihedral angles about the C−C bonds are, for ligand 1, O(1)−C(1)−C(2)−O(2) = −1(2)° and S(1)−C(1)−C(2)−S(2) = −4(1)°, and, for ligand 3, O(5)−C(5)−C(6)−O(6) = 6(2)° and S(5)−C(5)−C(6)−S(6) = 3(1)°. Due to the unsatisfactory result of the refinement of the atoms C(4), S(4), and O(4) (all within ligand 2), which showed unexpectedly high displacement parameters, the corresponding bond distances and angles from ligand 2 deviate significantly from the mean obtained from ligands 1 and 3 only (compare with data in the Experimental Section). The mean lengths for ligands 1 and 3 are S−C = 1.691(12), C−C = 1.560(15), and C−O = 1.230(14) Å. These values lie within the expected ranges and compare well with those determined in $CaK[Co(dto)_3]\cdot 4H_2O$ [S−C = 1.710(8), C−C = 1.516(23), and C−O = 1.226(8) Å].[20] The C−O (nonligating) length given above is close to those found here for the bridging mode toward Na. This fact indicates the rather

(20) Butler, K. R.; Snow, M. R. *Acta Crystallogr.* **1975**, *B31*, 354.

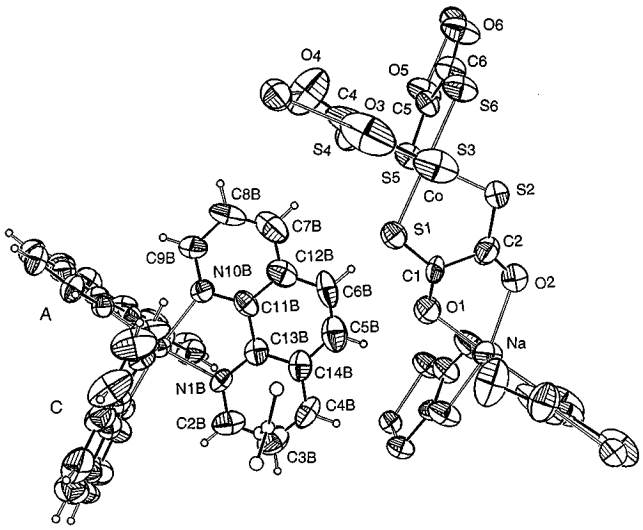

Figure 6. ORTEP picture (50% probability level) with the labeling scheme of the asymmetric unit of $[Ni^{II}(phen)_3][NaCo^{III}(dto)_3]\cdot C_3H_6O$ (**5**). H-atoms and acetone are shown as spheres of arbitrary size. The Co atom is hidden by S(3).

weak covalent bonding character of the oxygen atoms toward the sodium atom. For instance, the C−O (ligating) length for the oxalate ligand bound to iron(III) shows a mean value of 1.278(4) Å.[1]

The geometry around the cobalt center is best described by comparing it with the above cited mononuclear, tris-chelated $[Co(dto)_3]^{3-}$ compound.[20] Thereby, the effects which originate from the 3D connectivity within the network will be apparent. The mean Co−S length determined from ligands 1 and 3 is 2.244(4) Å, which is exactly the same as the value quoted for the mononuclear compound [2.244(5) Å].[20] Also the intraligand S−Co−S angles with values of 89.4(1)° and 89.9(1)° for the ligands 1 and 3 compare well with the average of 89.7(2)° given for the reference structure.[20] In addition inspection of Table 5 will show the interligand S−Co−S angles and thereby reveal the extend of the angular distortion of the CoS_6 core. For a comparison, the angular deviations around the metal cores for the cubic, heterometallic oxalate-bridged compounds[2] are all less than 10° from the idealized 90° or multiples there of.

The interatomic Na−O distances with a mean value of 2.376(11) Å for ligands 1 and 3 can be compared with the mean value of 2.319(3) Å in the oxalate-bridged network $[NaFe^{III}(ox)_3]_n^{2n-}$.[2] Furthermore, this distance is only slightly less than the sum of the corresponding ionic radii.

The $[Ni(phen)_3]^{2+}$ cations display bond distances and angles within normal limits.[21] Similar to the cation packing arrangement in the cubic oxalate-bridged compounds (**1**−**4**), three adjacent cations with their V-shaped pockets form a sufficiently large cavity to accommodate additional molecules. As noted above, no water molecules have yet been found to occupy these vacancies in the 3D structures but in the present case, using a water/acetone solution during the synthesis, an acetone molecule is now hosted in each cavity. Figure 7 depicts this vacancy which is now less symmetrical and more open than those found in the cubic compounds. The Ni−Ni distances between the three cations forming the cavity show a mean value of 10.42 Å. For comparison, the analogous Cr−Cr distance in compound **2** is 9.53 Å.

Figure 8 displays the three main projections of the network together with the corresponding cation arrangement. These projections manifest a close similarity to those of the oxalate-bridged compounds,[1,2] but at the same time show an obvious lowering in symmetry. Altogether, the flexibility of the 10-gon framework toward distortion is clearly elucidated.

Table 4. Fractional Coordinates ($\times 10^4$) and Equivalent Isotropic Displacement Parameters ($Å^2 \times 10^3$) for **5**

	x	*y*	*z*	$U_{(eq)}$[a]/$U_{(iso)}$[b]
Co	5821(1)	1188(1)	9192(1)	48(1)
S(1)	5726(2)	2562(2)	9181(2)	54(1)
S(2)	4482(2)	1107(2)	8908(2)	77(1)
S(3)	5591(3)	1121(2)	10399(2)	93(1)
S(4)	7186(2)	1333(3)	9440(2)	87(1)
S(5)	6209(2)	1284(2)	8023(1)	54(1)
S(6)	5912(2)	−197(2)	9124(2)	66(1)
C(1)	4810(6)	2780(7)	8806(7)	57(3)
C(2)	4171(7)	2061(7)	8691(7)	62(3)
O(1)	4598(5)	3489(5)	8621(8)	112(4)
O(2)	3503(5)	2267(5)	8434(5)	75(3)
C(3)	6611(8)	1152(7)	10791(6)	69(4)
C(4)	7165(11)	1164(9)	10156(12)	183(7)
O(3)	6735(9)	1155(7)	11453(5)	135(5)
O(4)	8024(7)	1043(9)	10556(6)	130(5)
C(5)	6384(7)	298(6)	7735(5)	48(3)
C(6)	6263(8)	−423(7)	8273(6)	59(3)
O(5)	6590(6)	128(4)	7112(4)	70(3)
O(6)	6444(7)	−1108(5)	8051(5)	86(3)
Na	3261(3)	3721(3)	8204(2)	65(1)
Ni	8602(1)	6448(1)	8570(1)	44(1)
N(1A)	8788(5)	6526(5)	7448(5)	47(2)
C(2A)	8263(8)	6642(7)	6910(6)	67(4)
C(3A)	8504(10)	6730(8)	6200(6)	74(4)
C(4A)	9322(10)	6681(7)	6022(7)	74(4)
C(5A)	10789(8)	6492(7)	6443(7)	64(3)
C(6A)	11290(8)	6354(7)	6971(7)	64(3)
C(7A)	11566(7)	6113(7)	8285(7)	66(4)
C(8A)	11234(7)	6066(8)	8977(7)	64(3)
C(9A)	10394(6)	6163(7)	9080(6)	58(3)
N(10A)	9863(5)	6309(5)	8553(4)	43(2)
C(11A)	10206(6)	6341(6)	7862(6)	46(3)
C(12A)	11027(7)	6285(7)	7701(7)	57(3)
C(13A)	9594(6)	6483(6)	7275(5)	43(2)
C(14A)	9916(7)	6558(6)	6562(6)	55(3)
N(1B)	7309(5)	6465(5)	8478(5)	46(2)
C(2B)	6819(8)	7094(8)	8501(7)	69(4)
C(3B)	5950(9)	7011(9)	8369(8)	77(4)
C(4B)	5640(7)	6277(9)	8209(7)	72(4)
C(5B)	5897(9)	4779(9)	8036(7)	79(4)
C(6B)	6397(9)	4121(8)	8047(7)	75(4)
C(7B)	7806(11)	3590(9)	8225(8)	94(5)
C(8B)	8610(11)	3751(8)	8407(10)	111(6)
C(9B)	8885(8)	4558(7)	8521(9)	77(4)
N(10B)	8374(5)	5183(5)	8486(5)	53(2)
C(11B)	7569(8)	5023(7)	8349(6)	52(3)
C(12B)	7255(9)	4238(8)	8206(7)	66(4)
C(13B)	6993(7)	5708(7)	8332(5)	49(3)
C(14B)	6167(7)	5577(8)	8185(7)	62(4)
N(1C)	8624(5)	7736(5)	8707(5)	48(2)
C(2C)	8642(8)	8323(6)	8208(6)	60(3)
C(3C)	8583(10)	9147(7)	8381(8)	78(4)
C(4C)	8516(9)	9376(7)	9080(8)	76(4)
C(5C)	8519(9)	8973(9)	10382(8)	84(4)
C(6C)	8536(8)	8374(10)	10874(7)	87(5)
C(7C)	8592(10)	6835(11)	11181(7)	98(5)
C(8C)	8623(11)	6053(10)	10933(8)	99(5)
C(9C)	8624(9)	5925(8)	10195(6)	75(4)
N(10C)	8581(5)	6517(5)	9708(4)	45(2)
C(11C)	8591(7)	7316(7)	9943(6)	54(3)
C(12C)	8600(8)	7508(9)	10688(7)	69(4)
C(13C)	8601(7)	7952(7)	9426(6)	54(3)
C(14C)	8527(7)	8789(7)	9639(6)	59(3)
C(1L)	5990(22)	6197(11)	10923(9)	126(13)[b]
C(2L)	6133(24)	5449(15)	11369(18)	128(13)[b]
O(1L)	5852(32)	6701(21)	11379(19)	281(24)[b]
C(3L)	6108(32)	6536(27)	10187(14)	176(21)[b]

[a] $U_{(eq)}$ is defined as one-third of the trace of the orthogonalized $\mathbf{U}_{ij}$ tensor. [b] Isotropically refined atoms.

(21) Baggio, R. F.; Calvo, R.; Brondino, C.; Garland, M. T.; Atria, A. M.; Spodine, E. *Acta Crystallogr.* **1995**, *C51*, 382.

Table 5. Selected Bond Lengths (Å) and Angles (deg) for **5**[a]

	Distances		
Ni−N(1A)	2.088(9)	Ni−N(10B)	2.091(9)
Ni−N(10A)	2.061(8)	Ni−N(1C)	2.105(8)
Ni−N(1B)	2.106(8)	Ni−N(10C)	2.095(8)
Co−S(1)	2.235(3)	Co−S(4)	2.276(4)
Co−S(2)	2.240(4)	Co−S(5)	2.244(3)
Co−S(3)	2.251(3)	Co−S(6)	2.256(3)
Na−O(1)	2.333(11)	Na−O(4)^{iii}	2.341(12)
Na−O(2)	2.429(9)	Na−O(5)^{iv}	2.369(9)
Na−O(3)^{iii}	2.564(14)	Na−O(6)^{iv}	2.372(9)
	Ligand 1		
S(1)−C(1)	1.676(12)	C(2)−O(2)	1.230(14)
S(2)−C(2)	1.675(12)	C(1)−C(2)	1.58(2)
C(1)−O(1)	1.248(14)		
	Ligand 2		
S(3)−C(3)	1.807(13)	C(4)−O(4)	1.59(2)
S(4)−C(4)	1.34(2)	C(3)−C(4)	1.47(2)
C(3)−O(3)	1.233(13)		
	Ligand 3		
S(5)−C(5)	1.708(10)	C(6)−O(6)	1.219(13)
S(6)−C(6)	1.704(11)	C(5)−C(6)	1.544(14)
C(5)−O(5)	1.223(12)		
C(1L)−O(1L)	1.19(2)	C(1L)−C(2L)	1.482(14)
C(1L)−C(3L)	1.47(2)		
	Angles		
N(10A)−Ni−N(10B)	93.9(3)	N(1A)−Ni−N(1C)	93.2(3)
N(10A)−Ni−N(1A)	81.2(3)	N(10C)−Ni−N(1C)	80.1(3)
N(10B)−Ni−N(1A)	90.7(4)	N(10A)−Ni−N(1B)	172.2(3)
N(10A)−Ni−N(10C)	92.1(3)	N(10B)−Ni−N(1B)	80.2(3)
N(10B)−Ni−N(10C)	97.1(4)	N(1A)−Ni−N(1B)	93.7(3)
N(1A)−Ni−N(10C)	170.1(3)	N(10C)−Ni−N(1B)	93.7(3)
N(10A)−Ni−N(1C)	95.4(3)	N(1C)−Ni−N(1B)	90.8(3)
N(10B)−Ni−N(1C)	170.4(3)		
S(1)−Co−S(2)	89.37(13)	S(5)−Co−S(6)	89.87(12)
S(1)−Co−S(5)	86.65(12)	S(3)−Co−S(6)	90.98(14)
S(2)−Co−S(5)	93.08(14)	S(1)−Co−S(4)	88.1(2)
S(1)−Co−S(3)	92.63(14)	S(2)−Co−S(4)	176.8(2)
S(2)−Co−S(3)	93.8(2)	S(5)−Co−S(4)	84.88(13)
S(5)−Co−S(3)	173.1(2)	S(3)−Co−S(4)	88.2(2)
S(1)−Co−S(6)	176.30(13)	S(6)−Co−S(4)	92.9(2)
S(2)−Co−S(6)	89.56(14)		
O(4)^{iii}−Na−O(1)	81.9(5)	O(6)^{iv}−Na−O(2)	104.5(3)
O(4)^{iii}−Na−O(6)^{iv}	163.7(5)	O(5)^{iv}−Na−O(2)	164.2(4)
O(1)−Na−O(6)^{iv}	98.6(4)	O(4)^{iii}−Na−O(3)^{iii}	65.8(4)
O(4)^{iii}−Na−O(5)^{iv}	95.6(4)	O(1)−Na−O(3)^{iii}	146.2(4)
O(1)−Na−O(5)^{iv}	98.1(3)	O(6)^{iv}−Na−O(3)^{iii}	115.1(4)
O(6)^{iv}−Na−O(5)^{iv}	68.1(3)	O(5)^{iv}−Na−O(3)^{iii}	94.8(4)
O(4)^{iii}−Na−O(2)	90.9(5)	O(2)−Na−O(3)^{iii}	100.9(4)
O(1)−Na−O(2)	68.6(3)		
	Ligand 1		
C(1)−S(1)−Co	106.0(4)	O(2)−C(2)−C(1)	115.6(10)
C(2)−S(2)−Co	107.1(4)	O(2)−C(2)−S(2)	127.4(10)
O(1)−C(1)−C(2)	117.6(10)	C(1)−C(2)−S(2)	117.0(8)
O(1)−C(1)−S(1)	123.5(9)	C(1)−O(1)−Na	119.7(8)
C(2)−C(1)−S(1)	118.9(9)	C(2)−O(2)−Na	118.2(8)
	Ligand 2		
C(3)−S(3)−Co	103.9(4)	S(4)−C(4)−C(3)	143(2)
C(4)−S(4)−Co	98.6(8)	S(4)−C(4)−O(4)	117.1(10)
O(3)−C(3)−C(4)	133(2)	C(3)−C(4)−O(4)	100(2)
O(3)−C(3)−S(3)	122.9(12)	C(3)−O(3)−Na^{i}	113.6(11)
C(4)−C(3)−S(3)	104.1(11)	C(4)−O(4)−Na^{i}	125.1(9)
	Ligand 3		
C(5)−S(5)−Co	106.1(4)	O(6)−C(6)−C(5)	116.5(10)
C(6)−S(6)−Co	106.7(4)	O(6)−C(6)−S(6)	125.7(9)
O(5)−C(5)−C(6)	117.6(9)	C(5)−C(6)−S(6)	117.8(8)
O(5)−C(5)−S(5)	123.0(8)	C(5)−O(5)−Na^{ii}	118.3(7)
C(6)−C(5)−S(5)	119.4(7)	C(6)−O(6)−Na^{ii}	118.7(7)
O(1L)−C(1L)−C(3L)	114(3)	C(3L)−C(1L)−C(2L)	143(3)
O(1L)−C(1L)−C(2L)	102(3)		

[a] Symmetry transformations used to generate equivalent atoms: (i) $x + 1/2, -y+1/2, -z + 2$; (ii) $-x + 1, y - 1/2, -z + 3/2$; (iii) $x - 1/2, -y + 1/2, -z + 2$; (iv) $-x + 1, y + 1/2, -z + 3/2$.

Photophysical Properties of $[Cr^{III}(bpy)_3][ClO_4][NaCr^{III}(ox)_3]$ (1) and $[Rh^{III}:Cr^{III}(1\%)(bpy)_3][ClO_4][NaCr^{III}(ox)_3]$. Absorption Spectrum. Figure 9 shows the unpolarized single-crystal absorption spectrum of **1** at 15 and 295 K (the cubic space group $P2_13$ gives no polarization information). It consists of a comparatively intense broad band centered at 18 300 cm^{-1} (ϵ_{max} = 90 L/(mol cm)) and a series of weaker, sharp lines mostly on the low-energy side of this band. The latter are reproduced in detail in Figure 10. Above 22 000 cm^{-1}, there is a rise to a very intense absorption band.

The molecular trigonal axis for both chromophores, $[Cr(bpy)_3]^{3+}$ and $[Cr(ox)_3]^{3-}$, whereby the latter is formally taken as a subunit of the infinite array, is preserved in the site symmetry of the crystal. Thus, for $[Cr(bpy)_3]^{3+}$, absorption energies and zero-field splittings are expected to be similar to those observed for this chromophore in other trigonal environments. The same holds for $[Cr(ox)_3]^{3-}$. As the spectra for both $[Cr(bpy)_3]^{3+}$ [22,24] and $[Cr(ox)_3]^{3-}$ [23] are well-known, the assignment of the bands is straightforward. With extinction coefficients below 100 L/(mol cm), all the bands below 21000 cm^{-1} are due to d−d transitions. The broad band at 18300 cm^{-1} definitely corresponds to the $^4A_2 \rightarrow {}^4T_2$ transition of $[Cr(ox)_3]^{3-}$. It directly gives the ligand field strength $10Dq$ = 18 300 cm^{-1}, which is a typical value for six-fold oxygen coordinated Cr(III).[25] The respective band for $[Cr(bpy)_3]^{3+}$ would be expected at energies around 23 000 cm^{-1}, as $10Dq$ for 6-fold nitrogen coordination is generally substantially larger.[25,26] As denoted in Figure 10, the band at the lowest energy, the doublet at 13 720 cm^{-1}, corresponds to the well-known R-lines of the $^4A_2 \rightarrow {}^2E$ transition of $[Cr(bpy)_3]^{3+}$. Its energy is close to the energy of 13 780 cm^{-1} of this transition in $[Cr(bpy)_3](PF_6)_3$,[22] and its zero-field splitting of 15 cm^{-1} is in the expected range.[24] The $^4A_2 \rightarrow {}^2E$ transition of $[Cr(ox)_3]^{3-}$, too, is easily identified as the doublet of sharp lines at 14 400 cm^{-1} by comparison with the 14 490 cm^{-1} reported for $[Cr(ox)_3]^{3-}$ doped $NaMg[Al(ox)_3]\cdot 8H_2O$.[23] The zero-field splitting in this case is 13 cm^{-1}. The shoulders on the low-energy side of this doublet may be assigned to the $^4A_2 \rightarrow {}^2T_1$ transition of $[Cr(bpy)_3]^{3+}$. The respective transition of $[Cr(ox)_3]^{3-}$ is found between 14 800 and 15 200 cm^{-1} together with some vibrational side bands, and the $^4A_2 \rightarrow {}^2T_2$ transition of $[Cr(ox)_3]^{3-}$ is found at 21 120 cm^{-1} (see Figure 9). As is usual for the (spin-forbidden) spin−flip transitions in Cr(III) complexes, they are all sharp, and as there is no center of inversion in tris-chelate complexes, most of the (electric dipole) intensity is in the electronic origins. Above 22 000 cm^{-1} the spectrum is swamped by the intense absorption of an LMCT transition of $[Cr(bpy)_3]^{3+}$.[26]

Luminescence and Energy Transfer. Figure 11a shows the luminescence spectrum of $[Cr^{III}(bpy)_3][ClO_4][NaCr^{III}(ox)_3]$ (**1**) at 20 K when irradiating at 568 nm, that is into the $^4A_2 \rightarrow {}^4T_2$ band of $[Cr(ox)_3]^{3-}$. The expected luminescence originating from the ^2E state of $[Cr(ox)_3]^{3-}$ is only seen as an extremely weak doublet at the same energy as the $^4A_2 \rightarrow {}^2E$ absorption. Despite the fact that $[Cr(bpy)_3]^{3+}$ does not absorb at the irradiation wavelength,[22] a much stronger luminescence, clearly originating from the ^2E state of $[Cr(bpy)_3]^{3+}$, appears at lower energy. Evidently, an efficient energy transfer process from the initially excited $[Cr(ox)_3]^{3-}$ chromophore as donor to $[Cr(bpy)_3]^{3+}$ as acceptor takes place. This is not surprising:

(22) Hauser, A.; Mäder, M.; Robinson, W. T.; Murugesan, R.; Ferguson, J. *Inorg. Chem.* **1987**, *26*, 1331.
(23) Schönherr, T; Spanier, J.; Schmidtke, H. H. *J. Phys. Chem.* **1989**, *93*, 5959.
(24) Riesen, H. *J. Lumin.* **1992**, *54*, 71.
(25) Schläfer, H. L.; Gliemann, G. *Einführung in die Ligandenfeldtheorie*, Akad. Verlagsgesellschaft: Frankfurt, Germany, 1967.
(26) König, E.; Herzog, S. *J. Inorg. Nucl. Chem.* **1970**, *32*, 585.

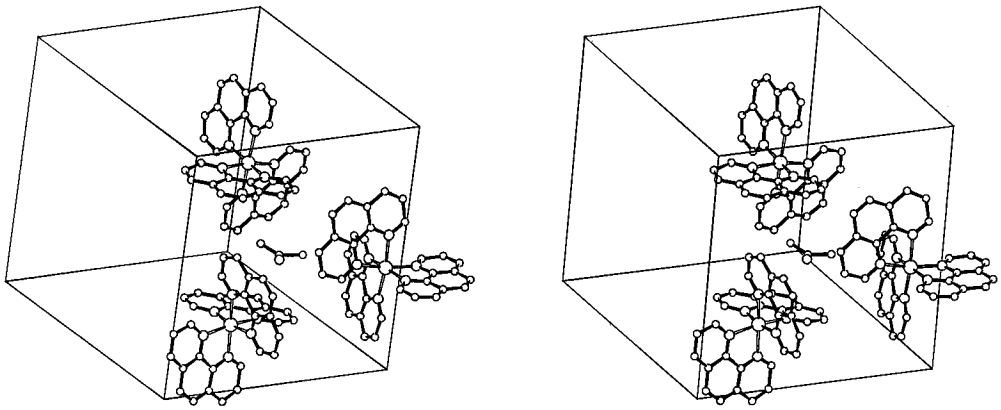

Figure 7. Stereoview of the $[Ni(phen)_3]^{2+}$ packing arrangement in the orthorhombic cell of compound **5** exhibiting the enlarged cavity with the accommodated solvent molecule.

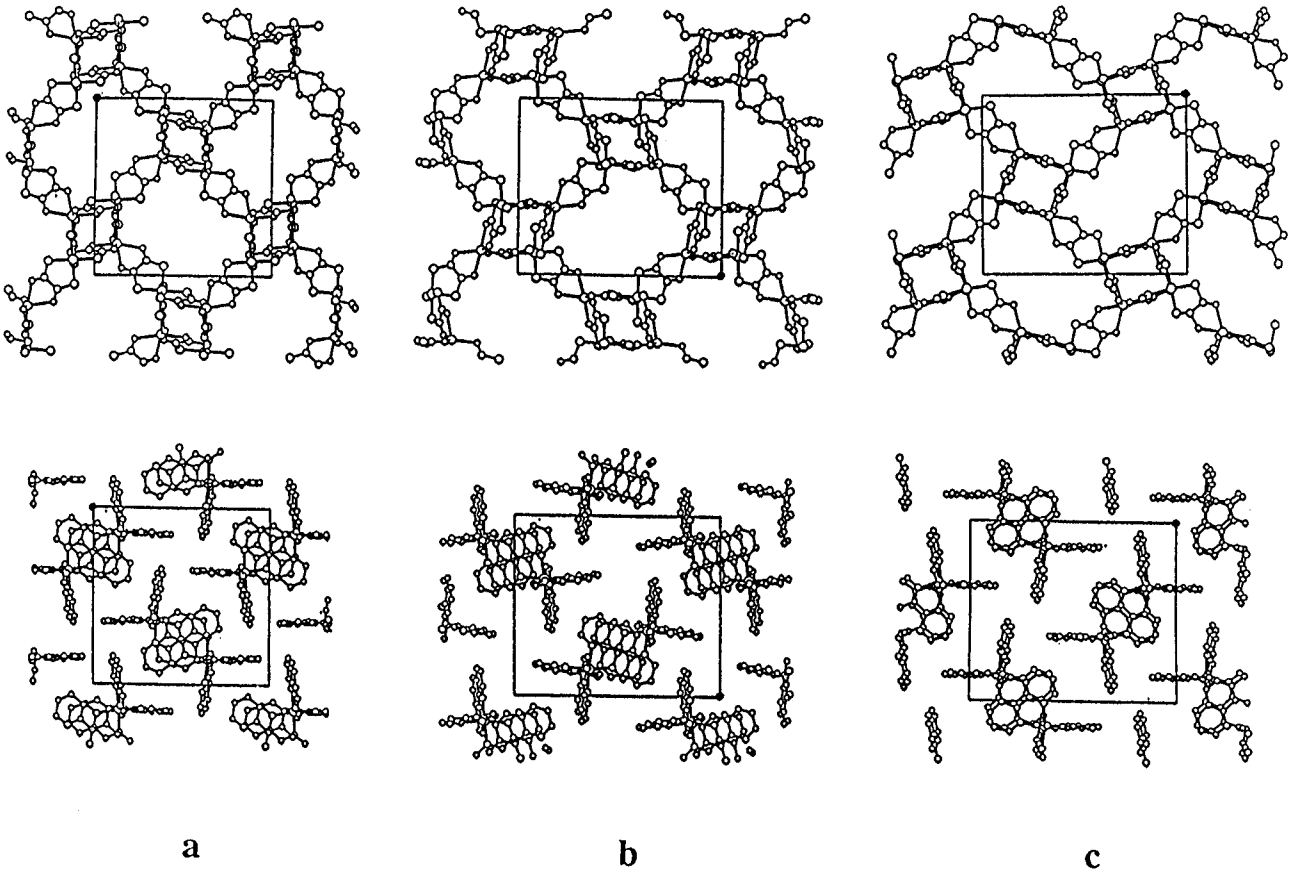

Figure 8. Three main projections (**a**, [001]; **b**, [100]; **c**, [010]) of the $[NaCo^{III}(dto)_3]_n^{2n-}$ network (**5**) in comparison with the situation of the $[Ni(phen)_3]^{2+}$ counterions.[31]

(a) the spectral overlap of the $^4A_2 \rightarrow {}^2E$ band of $[Cr(ox)_3]^{3-}$ and the $^4A_2 \rightarrow {}^2T_1$ band of $[Cr(bpy)_3]^{3+}$ allows for a resonant energy transfer process; (b) every $[Cr(ox)_3]^{3-}$ subunit is surrounded by seven $[Cr(bpy)_3]^{3+}$ complexes at distances between 6.1 and 9.2 Å. Unfortunately, the luminescence spectrum of the $[Cr(bpy)_3]^{3+}$ chromophore is rather complicated. As it should, the highest energy doublet of strong lines at 13 720 cm^{-1} coincides with the doublet which was assigned to the electronic origins of the $^4A_2 \rightarrow {}^2E$ transitions in absorption. Its temperature dependence, too, is consistent with the zero-field splitting of 15 cm^{-1} (see inset, Figure 11a). But instead of being more or less a mirror image of the absorption, the spectrum has additional sets of equally strong lines. Such a behavior is a common phenomenon in concentrated materials and is prone to misinterpretation. Cr(III) complexes are well-known for their photochemistry. For instance, $[Cr(bpy)_3]^{3+}$ is substitutionally labile, and therefore, even the best of crystals will contain a nonnegligible number of photochemically induced defects at the $[Cr(bpy)_3]^{3+}$ sites. Since resonant or phonon-assisted energy transfer within the ^2E state[27] of the $[Cr(bpy)_3]^{3+}$ system may be efficient down to low temperatures, these defects act as traps and give rise to so-called shallow trap emission.[28] That this is the case for **1** is borne out by the luminescence spectrum of $[Rh^{III}:Cr^{III}(1\%)(bpy)_3][ClO_4][NaCr^{III}(ox)_3]$ shown in Figure 11b. To begin with, there is now intense luminescence from the $[Cr(ox)_3]^{3-}$ chromophore, because the number of acceptors for the excitation energy on $[Cr(ox)_3]^{3-}$ is reduced. Secondly, as the energy transfer within the $[Cr(bpy)_3]^{3+}$ system is hindered in the doped system, the corresponding luminescence spectrum is now much simpler. The two origin lines now contain $\approx 90\%$ of the total $[Cr(bpy)_3]^{3+}$ luminescence, and their temperature dependence follows a Boltzmann distribution with an energy

(27) Imbush, G. F. In *Energy Transfer Processes in Condensed Matter*; DiBartolo, B., Ed.; NATO ASI B114: Plenum Press: New York, 1984.
(28) Blasse, G. *Philips Res. Rep.* **1969**, *24*, 131.

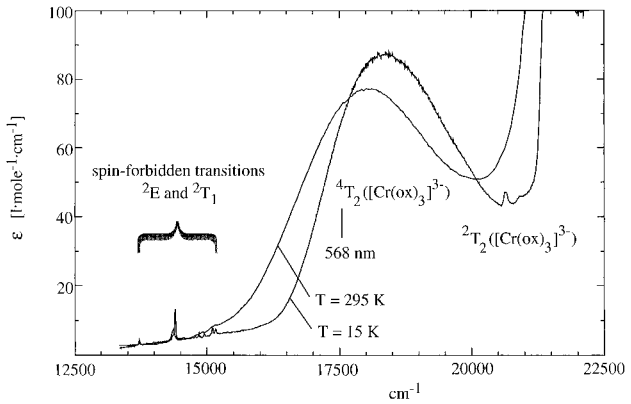

Figure 9. Single-crystal absorption spectrum of $[Cr^{III}(bpy)_3][ClO_4][NaCr^{III}(ox)_3]$ (**1**) at 15 and 295 K in the region of d−d transitions.

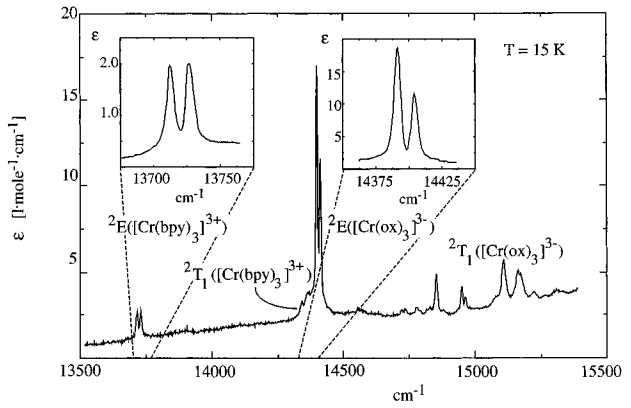

Figure 10. Detailed single−crystal absorption spectrum of $[Cr^{III}(bpy)_3][ClO_4][NaCr^{III}(ox)_3]$ (**1**) in the region of the spin-flip transitions $^4A_2 \rightarrow {}^2E$ and $^4A_2 \rightarrow {}^2T_1$, giving the assigments to the two Cr(III) chromophores as described in the text. Inset: Regions of electronic origins of the $^4A_2 \rightarrow {}^2E$ transitions enlarged.

difference of 15 cm^{-1}. This leaves no doubt as to the assignment of the ^2E state with a zero-field splitting of 15 cm^{-1}.

In concentrated $[Cr^{III}(bpy)_3][ClO_4][NaCr^{III}(ox)_3]$, the ratio of the integrated luminescence from $[Cr(ox)_3]^{3-}$ to the one from $[Cr(bpy)_3]^{3+}$ is $\approx 6 \times 10^{-5}$. Using this number as the quenching factor for the $[Cr(ox)_3]^{3-}$ luminescence, together with the rate constant for radiative decay $k_r \approx 700\ s^{-1}$ for isolated $[Cr(ox)_3]^{3-}$ complexes,[29] gives $k_{et} \approx 10^7\ s^{-1}$ as a rough estimate of the lower limit of the rate constant for the $[Cr(ox)_3]^{3-}$ to $[Cr(bpy)_3]^{3+}$ energy transfer.

Interestingly, in the diluted system the luminescence originating from $[Cr(ox)_3]^{3-}$ is still only ≈15% of the total luminescence, despite the low $[Cr(bpy)_3]^{3+}$ concentration. This is a clear indication that there is also efficient energy transfer within the $[Cr(ox)_3]^{3-}$ backbone.

Concluding Remarks

With this report, the flexibility of the already established 3D (10,3) network configurations toward a variation in the cationic site occupancy as well as toward a substitution of the oxalate, bridging ligands by 1,2-dithiooxalates has been demonstrated. Thereby, some new opportunities arise. On one side, the 1,2-dithiooxalate bridging ligands may offer an effective way to synthesize regularly alternating $[M_A^{II}M_B^{II}(ox)_3]_n^{2n-}$ frameworks. As a consequence, a dominant antiferromagnetic exchange interaction between adjacent metal ions would lead to a net spin moment, thus to an overall ferrimagnetic spin ordering. Work to examine these possibilities is in progress.

(29) Von Arx, M.; Diplomarbeit, University of Bern, 1995.

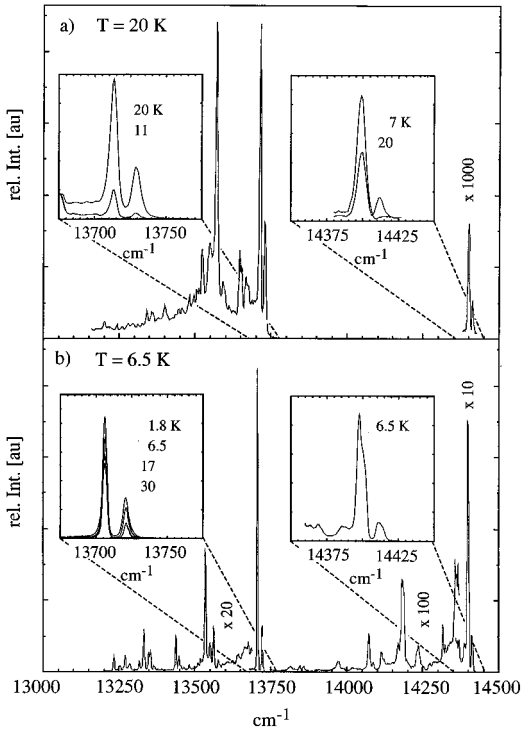

Figure 11. (a) Luminescence spectrum at 20 K of $[Cr^{III}(bpy)_3][ClO_4][NaCr^{III}(ox)_3]$ (**1**) (λ_{ex} = 568 nm). Inset: Blow-up of the regions of electronic origins at different temperatures. (b) Luminescence spectrum of $[Rh^{III}:Cr^{III}(1\%)(bpy)_3][ClO_4][NaCr^{III}(ox)_3]$ at 6.5 K (λ_{ex} = 568 nm). Inset: Blow-up of the regions of electronic origins at different temperatures.

On the other side, it is demonstrated that the 3D oxalate network structures possess interesting photophysical properties. The large variation with respect to the metal ions which can be incorporated and the numerous possibilities of combinations result in a diversity of photophysical processes. In the compounds $[Cr^{III}(bpy)_3][ClO_4][NaCr^{III}(ox)_3]$ (**1**) and $[Rh^{III}:Cr^{III}(1\%)(bpy)_3][ClO_4][NaCr^{III}(ox)_3]$, three efficient energy transfer processes have been identified: (i) resonant from the ^2E state of the initially excited $[Cr(ox)_3]^{3-}$ to the $[Cr(bpy)_3]^{3+}$ via the $^2T_1$ state of the latter, (ii) resonant or phonon-assisted within the ^2E state of $[Cr(bpy)_3]^{3+}$, and (iii) resonant or phonon-assisted within the ^2E state of $[Cr(ox)_3]^{3-}$. For more quantitative results, time resolved spectroscopic experiments will be necessary. In particular, the energy transfer within the oxalate backbone deserves further attention.[30]

Acknowledgment. Gratitude is expressed to the Swiss National Science Foundation for financial support under Project No. 21-39250.93 and 21-33184.92. The authors thank R. Eichenberger, University of Zürich, for assistance with the metal analysis and synthetic work.

Supporting Information Available: Tables of atomic fractional coordinates for hydrogen atoms (**1**, **5**) and for all atoms (**2**−**4**), bond lengths and angles (**2**−**4**), and anisotropic displacement parameters (**1**−**5**) and crystallographic data (**1**−**5**) (17 pages). Ordering information is given on any current masthead page.

IC950791J

(30) Hauser, A.; Riesen, H.; Pellaux, R.; Decurtins, S. Submitted for publication in *Chem. Phys. Lett.*

(31) SCHAKAL86, a Fortran program for the graphic representation of molecular and crystallographic models: Keller, E. *Chem. Unserer Zeit* **1986**, *20*, 178.